# Supplementary Material

## 1 AMS SMPS data comparison

A linear regression between the calculated mass based on the SMPS measured particle volume and the total mass concentration measured by the AMS was derived. To derive a particle density we used the following specific densities: Organics: 1.6 g/cm³; ammonium nitrate: 1.73 g/cm³; ammonium sulfate: 1.77 g/cm³; sulfuric acid: 1.84 g/cm³. The average particle mass density for the whole campaign was 1.71 g/cm³. We used both the complete volume measured by the SMPS, and only up to $d_{mob}$ = 500nm which corresponds to a $d_{va}$ of about 855 nm where the AMS inlet starts to cut off significantly larger particles. $R^2$ is well below 0.1 in both cases, while the slope is 0.44 when including all SMPS data, and 0.46 when only using SMPS data up to 500 nm. The colour coding indicates that the relationship is poorer for lower particulate sulfate concentrations, and seems to be partly due to non-refractory particles such as sea salt contributions (see colour coding by the PIKA derived sea salt species). Based on the low $R^2$ values and available literature (Middlebrook et al. 2012) we decided to use CE = 0.5. CE = 0.5 can be interpreted as the upper envelop (see Figure S1).

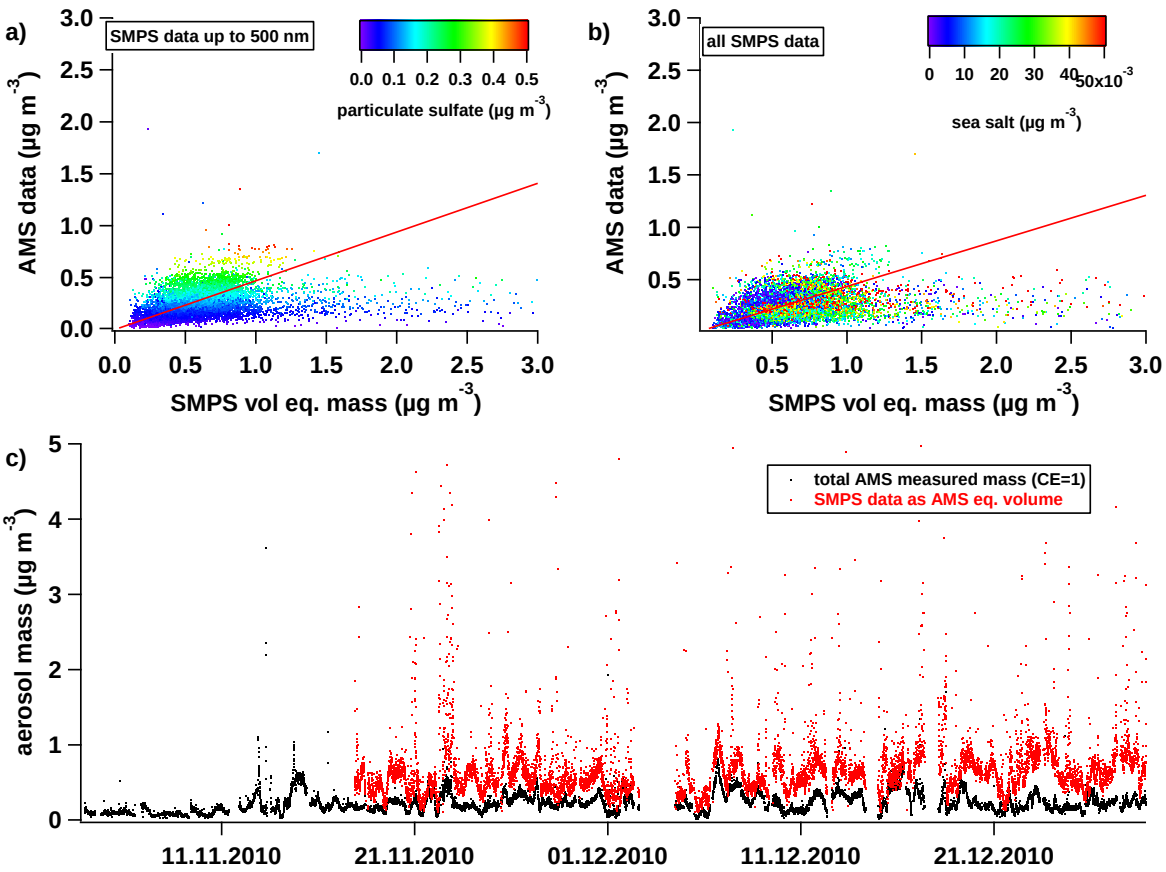


Figure S1: AMS aerosol mass versus SMPS volume equivalent mass for a) SMPS data up to 500 nm $d_{mob}$ and b) for all SMPS data. c) Time series of AMS aerosol mass versus SMPS volume equivalent mass data. Note that the AMS data is not corrected for sea salt after Ovadnevaite et al. (2012) by upscaling m/z 57.95 (Na35Cl+) by a factor of 51.

## 2 AMS sea salt detection

Following the BI field campaign, additional laboratory measurements were undertaken with a different AMS (compact time-of-flight aerosol mass spectrometer as described by Schmale et al. (2010)) to characterise the extent to which the AMS is capable of sea salt quantification and identify potential cross-sensitivities to other AMS standard chemical species. Known amounts of NaCl and sea salt (SIGMA-Aldrich sea salt standard S9883), each mixed separately with ammonium nitrate in solution, were measured with the AMS across a range of vapouriser temperatures between 480 and 720 °C. The ratios of two NaCl and sea salt fragments, $Na^+$ (*m/z* 23) and $NaCl^+$ (*m/z* 58), and the AMS species chloride (based on the standard fragmentation table) to nitrate were characterized.

For the NaCl solution, the ratio of *m/z* 58 and *m/z* 23 to $NO_3^-$ increased linearly with temperature ($R^2 = 0.94$, slope $4.7 \times 10^{-5}$, and $R^2 = 0.99$, slope $6.4 \times 10^{-4}$, respectively, see Fig. S2, bottom panel). The same *m/z* ratios behaved differently for the sea salt solution for which the response was non-linear: While the ratio *m/z* 58 to $NO_3^-$ peaked near 550 °C, the *m/z* 23 to $NO_3^-$ ratio increased steadily but not linearly with temperature (see Fig. S2). These different behaviours of the $Na^+$ and $NaCl^+$ ions in the SIGMA-Aldrich sea salt solution have also been reported by Ovadnevaite et al. (2012). Those authors argue that either the fragmentation of $NaCl^+$ ions increases at higher vapouriser temperatures, leading to lower ion concentration, or the ion thermal velocity increases resulting in a lower detection efficiency. For $Na^+$ the increasing concentration with higher temperatures is assumed to be related to higher fragmentation of the $NaCl^+$ ion and partly to surface ionisation. In addition, the different behaviours of the two ions as a function of the salt solution suggest that the AMS vapourisation and ionisation processes are significantly influenced by the mixture of salts. Deriving a scaling factor based on these fragments would thus lead to a highly uncertain quantification for sea salt on Bird Island, especially since the contributing salts in ambient marine air are largely unknown and likely to vary strongly depending on the location (e.g., BI aerosol is influenced strongly by $NH_3$ emissions). Indeed, unpublished measurements revealed significant differences in properties (hygroscopic growth, crystallisation etc.) of reference sea salts from different suppliers, further emphasising the influence of trace metals on its physicochemical behaviour (C. Braban, pers. comm.).

While there was a large discrepancy of a factor greater than 2 for $NaCl^+$ and $Na^+$ ions in the scaling factor between pure NaCl and sea salt standard at 600 °C, for chloride the results were

more consistent, ranging between a factor of $3.15 \pm 0.20$ and $3.97 \pm 0.14$ across all experiments. However, up-scaling based on AMS chloride might lead to errors for at least two reasons: (1) particulate chloride concentrations might not be quantified correctly by AMS measurements as it forms salts that have relatively high vapourisation temperatures (> 600 °C), and (2) other sources beside sea salt might contribute to the overall chloride concentration.

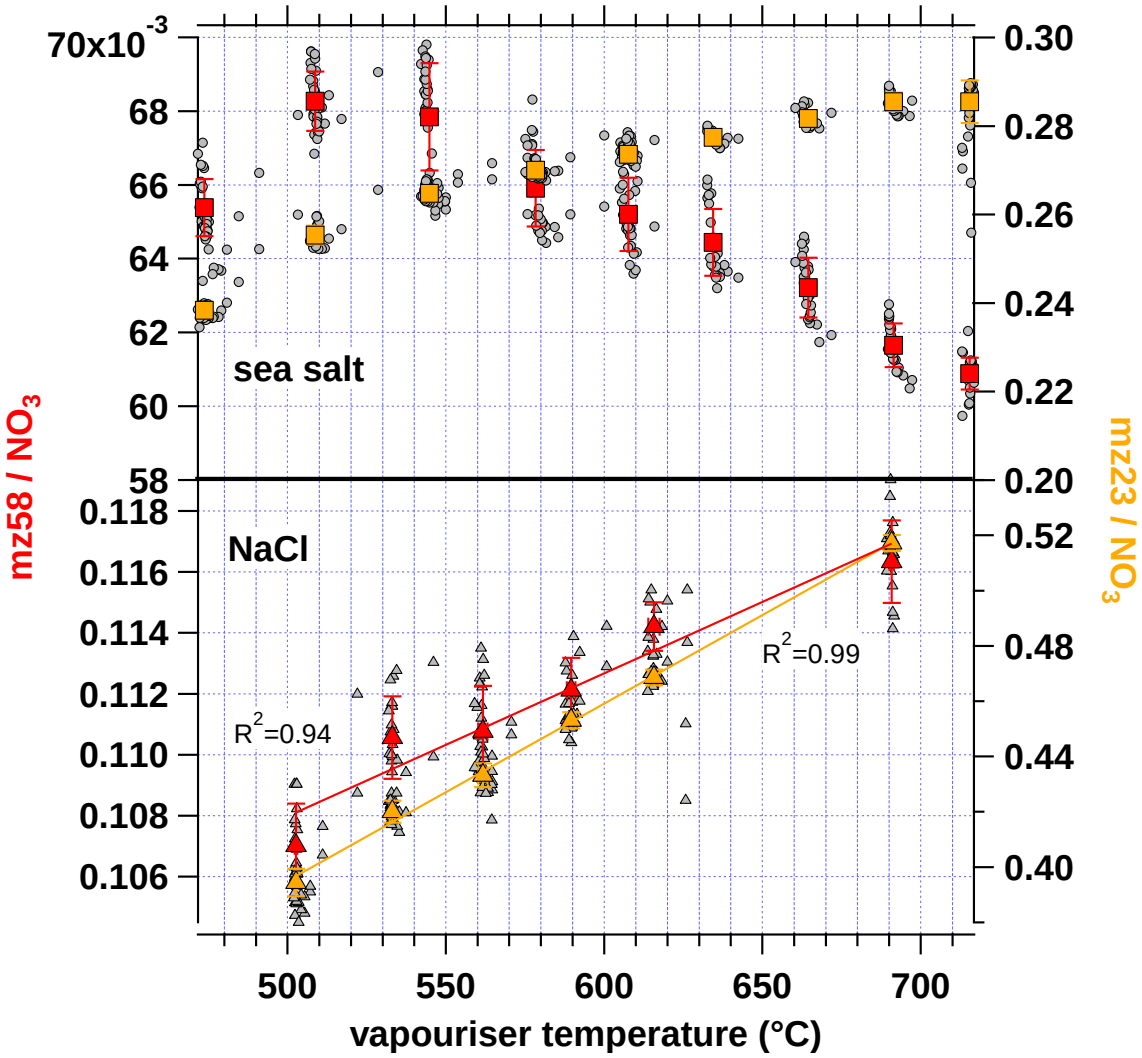


Figure S2: Ratios of *m/z* 58 ($NaCl^+$) and *m/z* 23 ($Na^+$) over particulate nitrate for a solution of standard sea salt (SIGMA-Aldrich S9883, upper panel) with ammonium nitrate (mass ratio 0.9) and for a solution of pure NaCl (lower panel) with ammonium nitrate (mass ratio 1.1) as function of vapouriser temperature. The slope of the linear regression of m/z58 over particulate nitrate versus the heater temperature is $4.73*10^{-5}$, the slope of m/z23 over particulate nitrate versus the heater temperature is $6.38*10^{-4}$.

## 3 Weighting *m/z* 29 for PMF analysis

Since it was not clear whether the signal at *m/z* 29 was partly an artefact due to a leakage in the vacuum chamber, this mass to charge ratio was downweighted. Given the case of a leakage, more air molecules would be available to produce a signal predominantly at *m/z* 28 ($N_2^+$). This would result in an elevated baseline influencing the neighbor *m/z* 29 which in turn would be overestimated.

When not downweighting *m/z* 29 a six factor PMF solution seemed to best meet the criteria of a minimum $Q/Q_{exp}$. However, one factor mainly consisting of *m/z* 29 (62.3 %) and *m/z* 44 (9.5 %) was derived. This factor, based on only two mass to charge ratios and based to more than 50 % on *m/z* 29 was not trusted, due to steps in the signal intensity occurring in the time series (see Fig. S3). To test whether this factor might be an artefact, *m/z* 29 was downweighted by a factor 100 and 1000. The factor profile disappeared when downweighting by either factor. Table S1 shows the relative differences between downweighting by a factor 100 or 1000 in the time series and mass spectra for the five factor solution at *fpeak* = 0 and *seed* = 0. For the final analysis *m/z* 29 was downweighted by a factor of 1000.

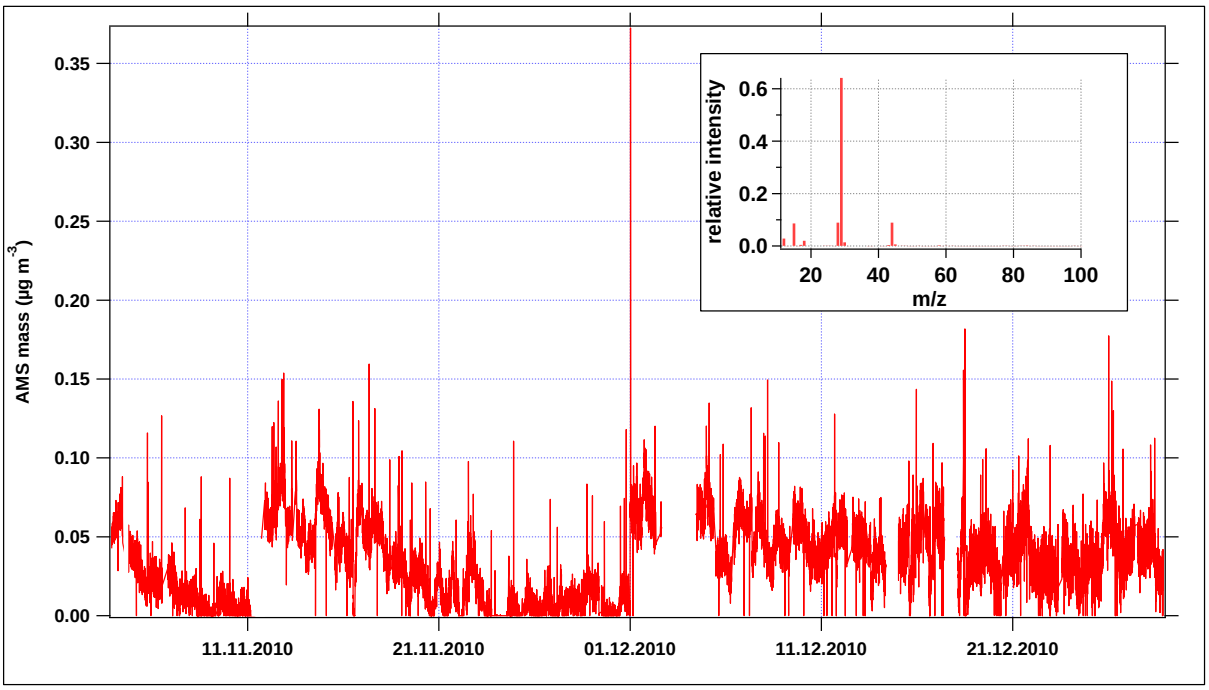


Figure S3: Time series and mass spectrum of the m/z 29 dominated factor

Table S1: Relative difference between downweighting m/z 29 by a factor 100 or 1000

| Factor | relative difference 100/1000 in mass spectra (%) | relative difference 100/1000 in time series (%) |
|---|---|---|
| MSA-OA | 2.15 | 0.36 |
| AA | 1.68 | 0.71 |
| M-OOA | 1.04 | 1.30 |
| SS-OA | 4.06 | 2.59 |
| HOA | 3.02 | 3.19 |

## 4 Key diagnostic plots for the PMF 5 factor solution

The change in slope of the $Q/Q_{exp}$ vs. the number of PMF solutions curve between factors 4 and 5 (see Fig. S4 a) indicates that at least 5 factors should be considered. The *Q* value or "PMF quality of fit parameter" (Zhang et al., 2011) refers to the sum of weighed square residuals. Five factors were chosen, because factor splitting was identified in the solutions using 6 or more factors (see Fig. S4). For example, factor 1 (count upwards from bottom) in the 5-factor solution is split into factors 1 and 2 in the 6-factor solution, as the time series clearly show (cf. Figs. S5c and S5e). Also, the correlation between the two mass spectra is very high at 99 % (not shown). In the 5-factor solution, factor 1 contributes 23.5 % of the mass, while factors 1 and 2 contribute 17.8 and 12.2 % in the 6 factor solution. The 7-factor solution yields factors that do not represent meaningful OA aerosol mass spectra, where e.g., *m/z* 28 and 44 make up 50 % of the mass. Choosing only 4 factors results in factors 3 and 5 from the five factor solution being merged. Factor 5 in the 5-factor solution was identified as hydrocarbon-like OA (HOA), based on the high correlation ($R^2$ = 0.92) with the reference mass spectrum (A-DEC-Q-015) of the AMS UMR database, based on Ng et al. (2011). When only 4 factors are chosen, the correlation to the HOA reference spectrum decreases to $R^2$ = 0.76. The additional profile in the 5-factor solution, which was identified as marine oxygenated OA (M-OOA), has a low correlation with the HOA reference spectrum ($R^2$ = 0.10), so that the separation of the factors is meaningful. Also, the time series of factors M-OOA and HOA have a correlation coefficient of $R^2$ = 0.12 (see Fig. S4 d), so that a 5-factor solution is plausible. All time series' correlation coefficients are in the range between -0.25 and 0.34 ($R^2$ between 0.06 and 0.12), while the mass spectrum R ranges between 0.14 and 0.59 ($R^2$ between 0.02 and 0.35). The relatively high correlations in the mass spectra between factors 1 and 2 as well as 2 and 3 (see Fig. S4 d) are based on the relatively high contributions of *m/z* 28, 29 and 44 to the signals. Other marker fragments, however, do not coincide.

The chosen final *fpeak* is 0, where $Q/Q_{exp}$ is at a minimum (see Fig. S4c). All other values of *fpeak* between -1 and 0.2 show only rotational ambiguity in the 5-factor solution, while *fpeak* > 0.2 introduces a factor consisting to 80 % of *m/z* 29, which does not represent a meaningful chemical mass spectrum. Fig. S4 f) shows that this factor starts to dominate the contributions to the total reconstructed mass of OA. Since Zhang et al. (2011) recommend running PMF for a range of *fpeaks* such that the range of $Q/Q_{exp}$ values is at least 3 % above the minimum $Q/Q_{exp,}$ and since this was not the case for the fpeak range -1 to 1, we additionally explored

the fpeak range between -5 and 5 in steps of one (Fig. S4 g) and h). However, no other more plausible was found in the larger range. The $Q/Q_{exp}$ value < 1 at *fpeak* = 0 indicates that the error matrix was somewhat overestimated which is consistent with downweighting *m/z* 29 by a factor of 1000. *Seed* 0 has been chosen to represent the final 5-factor solution, as $Q/Q_{exp}$ is very stable over the whole range of tested *seeds*. Also, the contribution of each factor to the total organic mass when varying *seeds* does not vary significantly (see Fig. S4b).

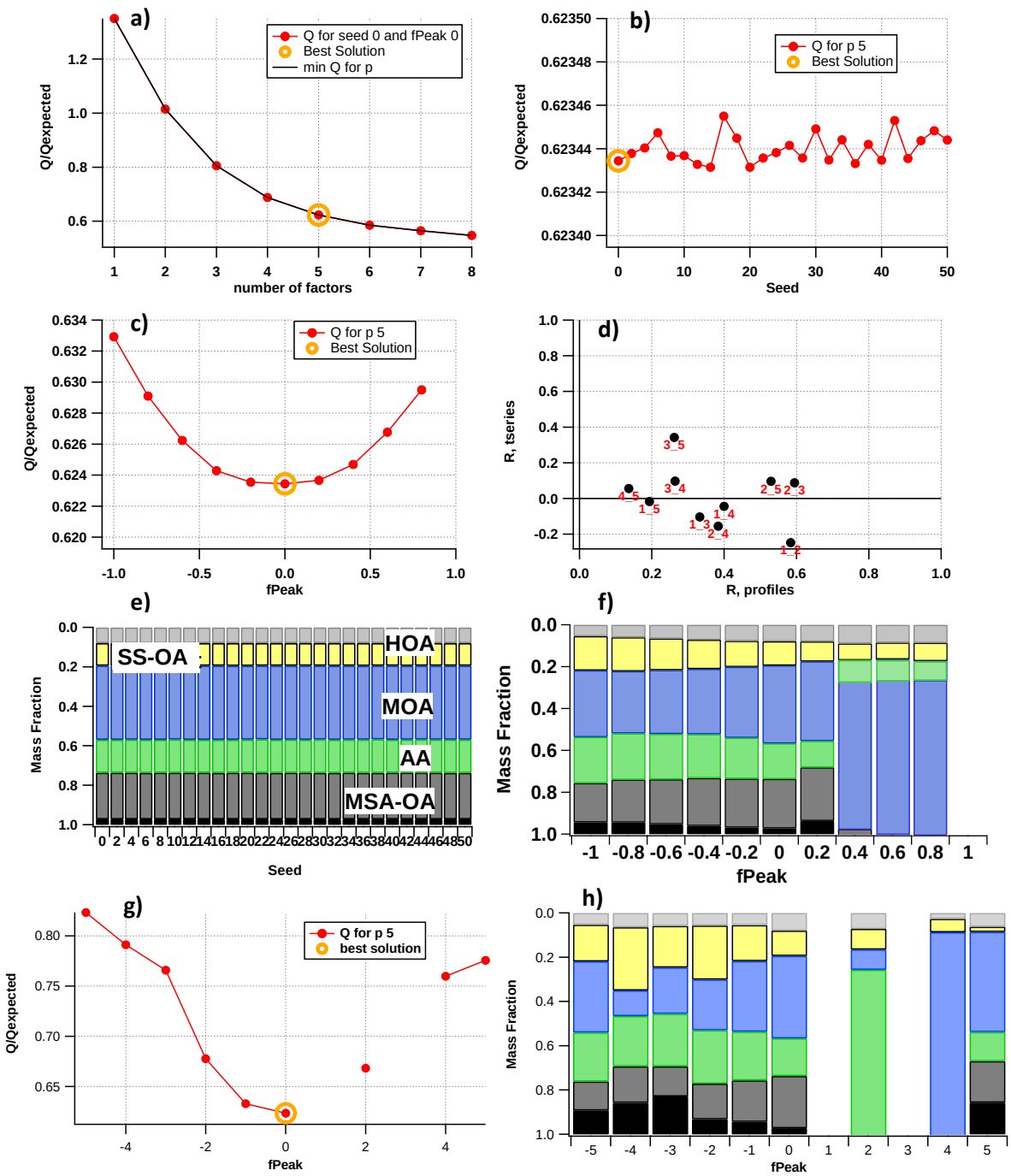

Figure S4: **a)** $Q/Q_{exp}$ as a function of the number of factors (*P*) used in the PMF analysis; the yellow circle denotes the best solution presented in this work **b)** $Q/Q_{exp}$ as a function of seeds between 0 and 50 in steps of two, **c)** $Q/Q_{exp}$ as a function of *fpeaks* between -1 and 1 in steps of 0.2, **d)** Pearson's correlation coefficient for time series and mass spectra for the 5 factor solution, **e)** variation of factor contributions to total OA as a function of *seeds*, **f)** variation of factor contributions to total OA as a function of *fpeaks*.

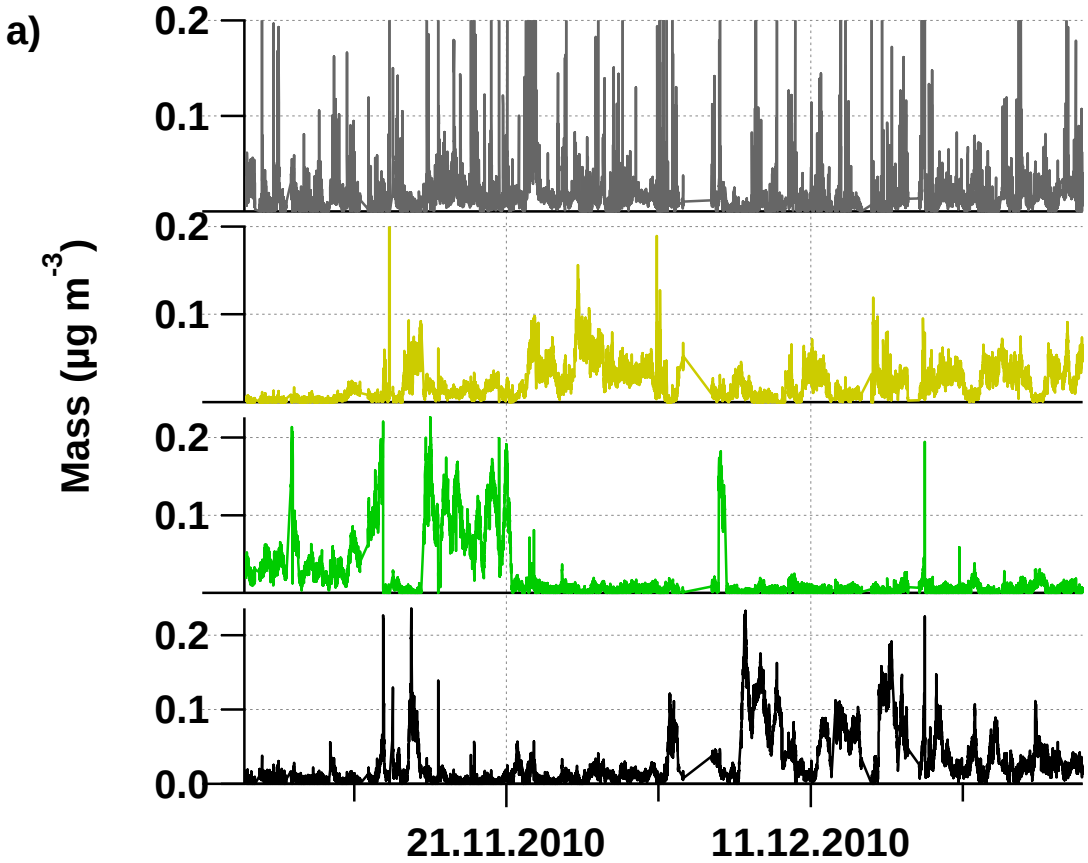
a)
Mass (µg m-3)
0.2
0.1
0.2
0.1
0.2
0.1
0.2
0.1
0.0
21.11.2010
11.12.2010

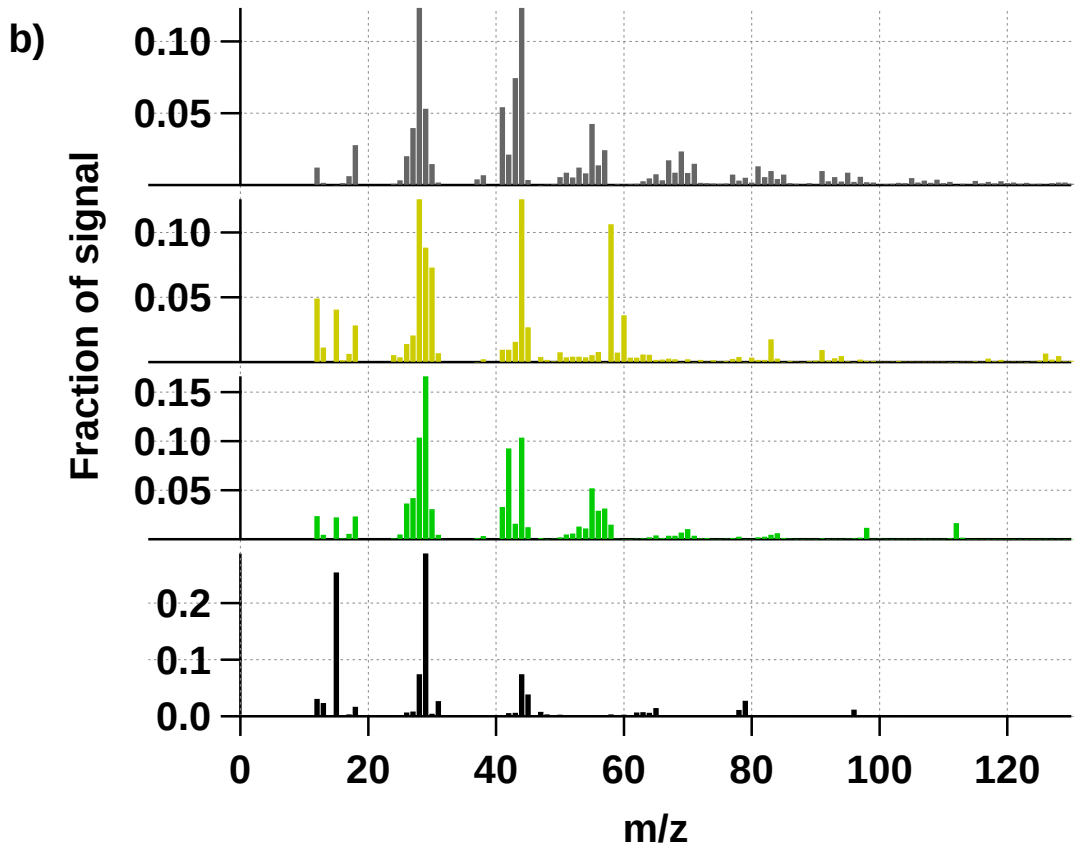
b)
Fraction of signal
0.10
0.05
0.10
0.05
0.15
0.10
0.05
0.2
0.1
0.0
0
20
40
60
80
100
120
m/z

146

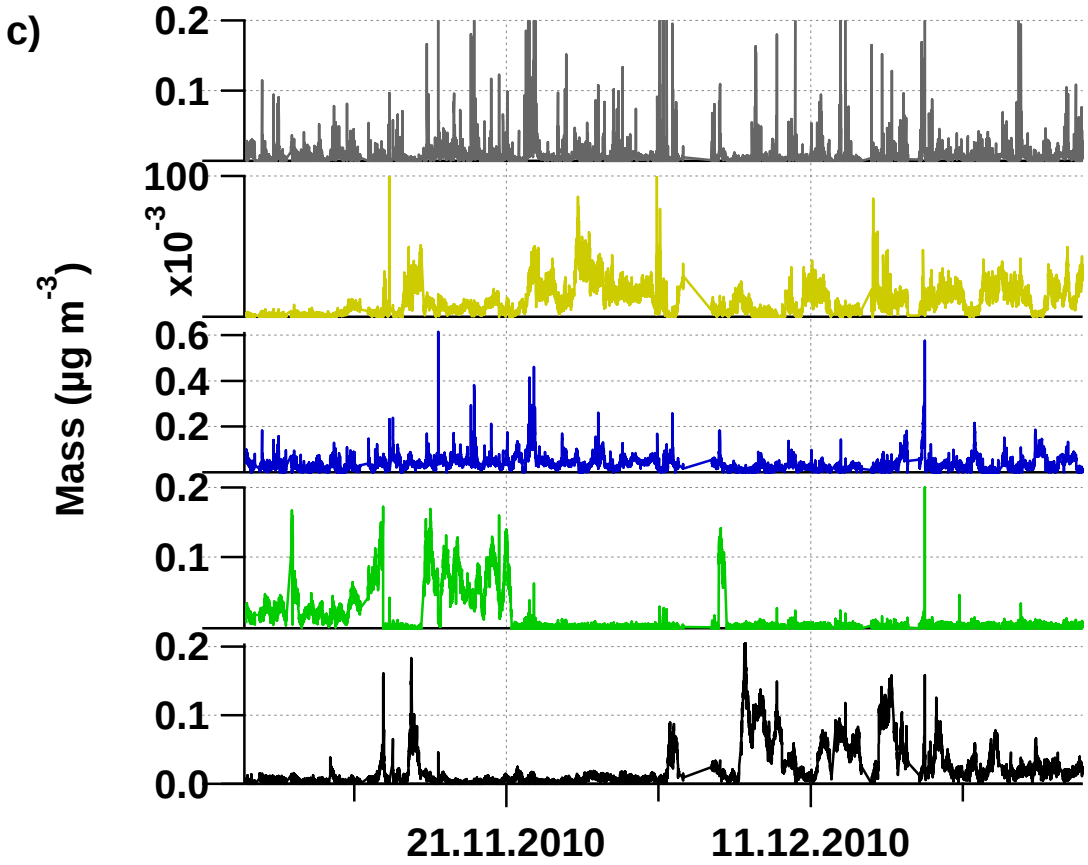
c)
Mass (µg m-3)
0.2
0.1
100
x10-3
0.6
0.4
0.2
0.2
0.1
0.2
0.1
0.0
21.11.2010
11.12.2010

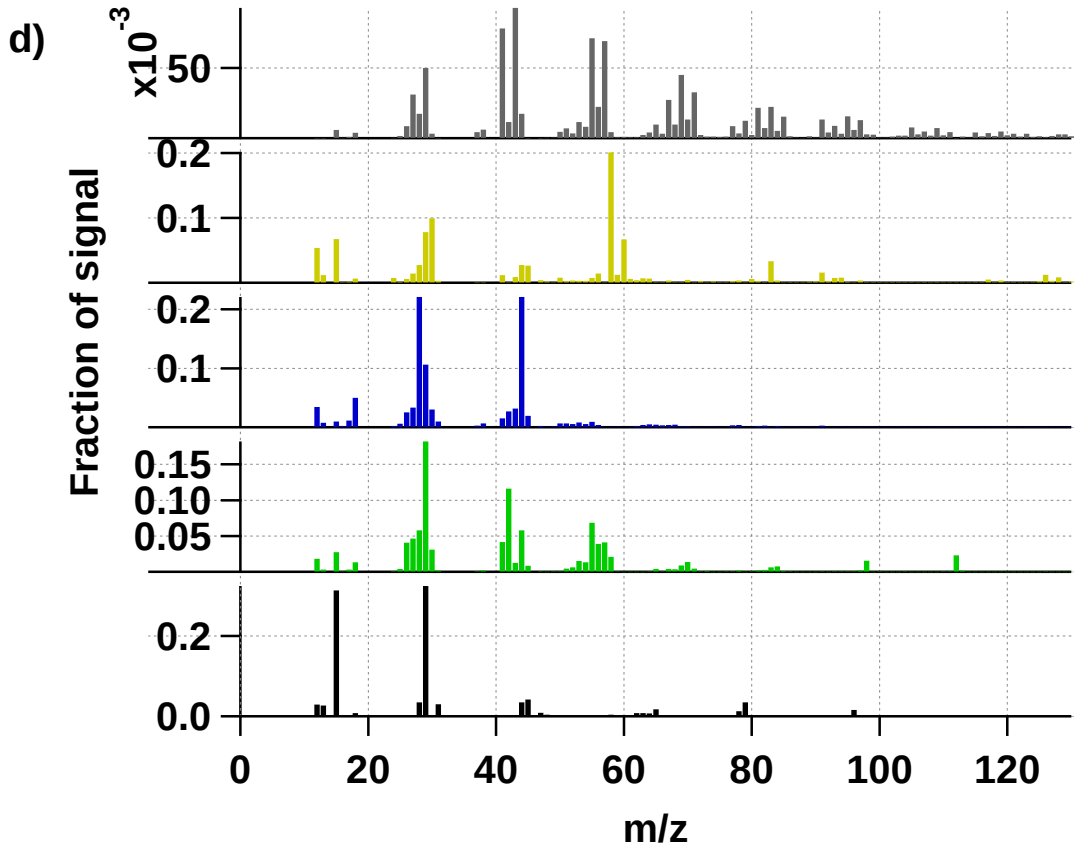
d)
Fraction of signal
x10-3
50
0.2
0.1
0.2
0.1
0.15
0.10
0.05
0.2
0.0
0
20
40
60
80
100
120
m/z

147

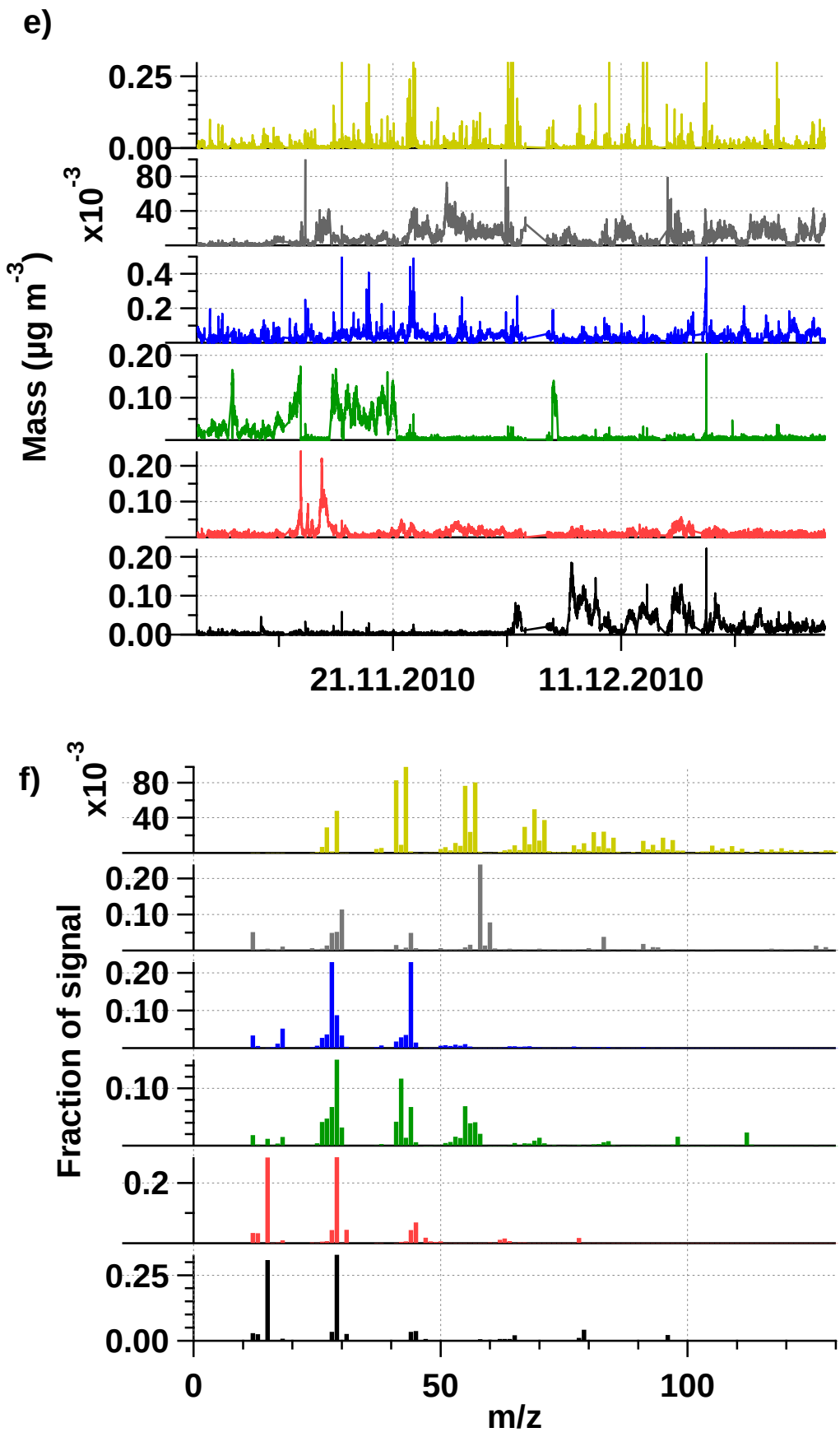


Figure S5: Comparison between the time series and mass spectra of the 4 (a,b), 5 (c,d) and 6 (e,f) factor PMF solutions

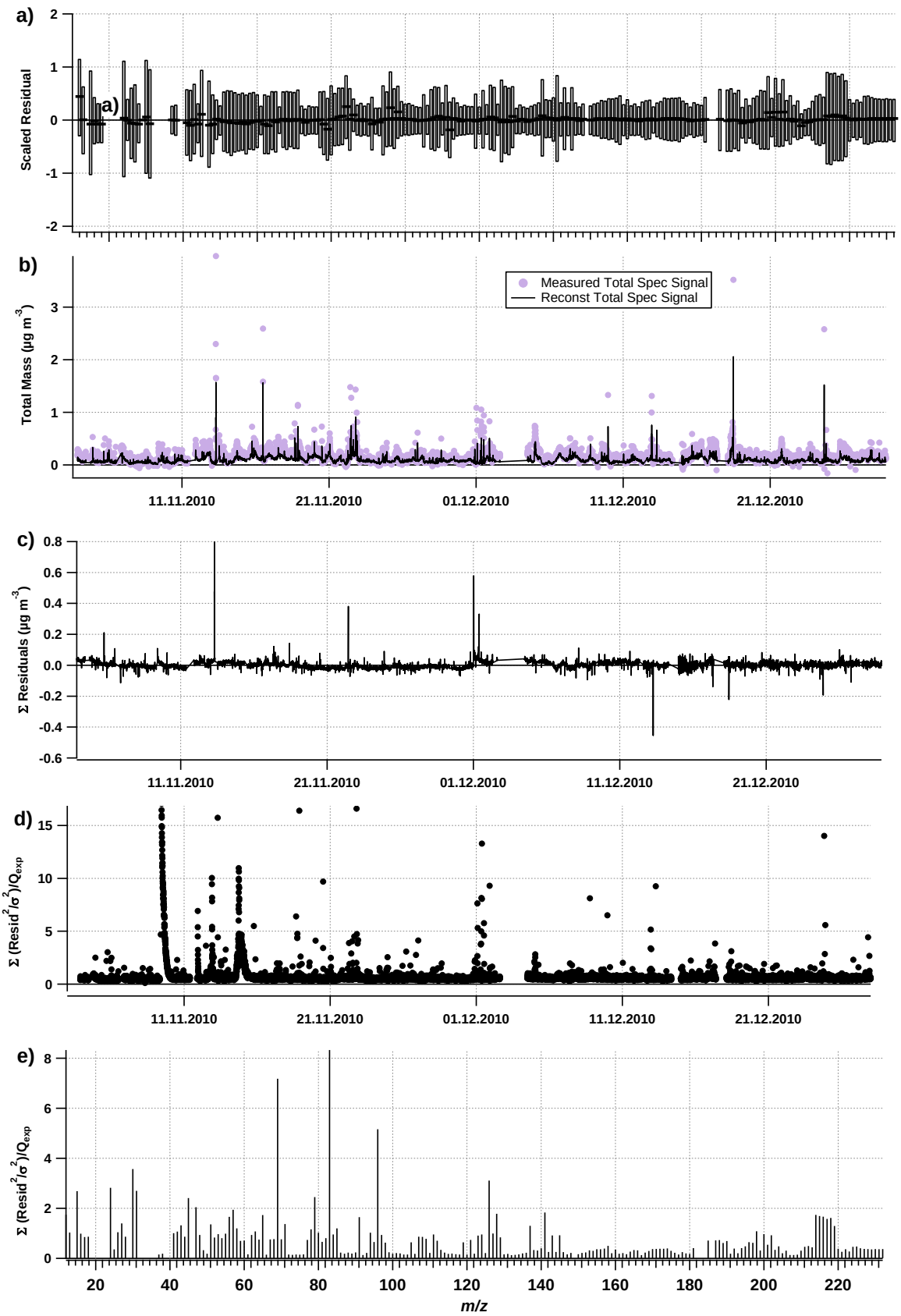


Figure S6: **a)** scaled residuals for each m/z, the horizontal bars indicate the median while the boxes represent the interquartile, **b)** comparison time series of the reconstructed OA (sum of

the five factors) and the measured OA, **c)** sum of the residuals (measured – reconstructed) of the fit, **d)** $Q/Q_{exp}$ for each time step, and **e)** $Q/Q_{exp}$ for each mass to charge ratio

## 5 Estimation of uncertainty of PMF results as a function of *fpeak* and *seeds* variations

For the mass spectrum averages only *m/z* between 12 and 130 were considered as heavier ion fragments were not significant contributors to the factors. All mass concentrations (at each *m/z* and at each point in time) that were smaller than 0.0001 µg $m^{-3}$ or greater than 1 µg / $m^3$ were excluded from the calculations. The low values add high uncertainties to the factors while the large values reflect peaks that may bias the results of the statistical analysis.

Table S2 shows the relative standard deviation from the mean for each factor in mass spectrum and time space for varied *fpeaks* and *seeds*. The *seed* variation has very little influence on the uncertainty of each individual factor. Factor 2 MS *seed* variation experiences the largest variability with 4.67 %. The *fpeak* variation however has larger influence on the stability of the factors for both time series and mass spectra. The variability ranges between 17 and 38 % with two extreme cases for factor 1 mass spectra (75.9 %) and factor 3 time series (130.17 %). The deviations in the factor 1 mass spectrum are mainly due to the variability in m/z 29 and 15 that make up 65 % of the total variability in this spectrum. The M-OOA factor is dominated by masses m/z 28 and 44 and 29 which can lead to high variability as these fragments contribute to all factors. In addition, for fpeaks greater than or equal to 0.4 M-OOA becomes the dominating factor (see Fig. S6 f) while for example, the MSA factor nearly disappears which is not a physically meaningful solution. This explains the large variability in the time series of different *fpeak* calculations.

Table S2: Relative standard deviations for each factor profile mass spectrum and time series based on the variations of *seeds* and *fpeaks* and based on the statistical variations through the bootstrapping method (all numbers in %).

| Factor | $seeds_{MS}$ | $seeds_{TS}$ | $fpeak_{MS}$ | $fpeak_{TS}$ | $Bootstrap_{MS}$ | $Bootstrap_{TS}$ |
|---|---|---|---|---|---|---|
| MSA-OA | 1.61 | 0.52 | 75.9 | 29.1 | 2.51 | 2.37 |
| AA | 4.67 | 0.80 | 28.2 | 31.9 | 3.56 | 2.59 |
| M-OOA | 0.54 | 0.69 | 37.4 | 130.2 | 7.92 | 4.26 |
| SS-OA | 1.15 | 0.40 | 29.1 | 15.3 | 16.1 | 7.26 |
| HOA | 0.19 | 0.90 | 16.5 | 14.5 | 13.5 | 9.19 |